EXTRACTION OF RITZ VECTORS FROM VIBRATION TEST DATA

Hoon Sohn

Engineering Sciences Applications Division, Engineering Analysis Group,
Los Alamos, National Laboratory, Los Alamos, NM 87545, U.S.A.
E-mail: sohn@lanl.gov

AND

Kincho H. Law

Department of Civil and Environmental Engineering, Stanford University, Stanford,
CA 94305–4020, U.S.A.

Modal parameters obtained from modal testing (such as modal vectors, natural frequencies, and damping ratios) have been used extensively in system identification, finite element model updating, and structural health monitoring. As an alternative to modal vectors, load-dependent Ritz vectors have been shown useful in various areas of structural dynamics such as model reduction and damage detection. The applications of Ritz vectors, however, have been mainly limited in analytical and numerical analyses because of the difficulty to identify them from vibration tests. This paper presents a procedure to extract load-dependent Ritz vectors using a complete flexibility matrix constructed from measured vibration test data. The proposed method cannot only construct the Ritz vectors corresponding to the actual load pattern employed in vibration tests, but also generate Ritz vectors from arbitrary load patterns. Experimental data obtained from the vibration test of a grid-type bridge structure are employed to validate and illustrate the proposed extraction procedure.

© 2001 Academic Press

1. INTRODUCTION

Modal parameters such as modal vectors, natural frequencies and damping have been widely employed in many fields of structural dynamics. For example, in numerical dynamic analysis, a multi-degree-of-freedom (mdof) system can be decoupled into a number of single-degree-of-freedom (sdof) systems using the orthogonality feature of modal vectors and the vibration response of the system can be approximated by the modal superposition of a small set of the sdof system responses. For vibration test, the response time histories are typically transformed into the frequency domain using a spectral analyzer and the test results are often presented in the form of modal parameters.

It has been shown that load-dependent Ritz vectors have many potential advantages in structural dynamics over modal parameters. For linear dynamic analyses, the response quantities of interest can be approximated more effectively by a smaller number of Ritz vectors than the modal vectors [1, 2]. In numerical analysis, Ritz (or Lanczos) vectors have been used to find partial extremal solutions of large eigenvalue problems [3] and to reanalyse a structural system with localised modifications [4]. In structural monitoring and damage diagnosis, numerical simulations have shown that Ritz vectors are able to identify damage better than modal vectors [5, 6]. For system identification and damage detection problems, however, the Ritz vectors need to be obtained from experimental test data.

Cao and Zimmerman were probably the first to attempt extracting Ritz vectors from measured vibration data using a state-space formulation [5]. In this paper, we present a new extraction procedure based on a complete flexibility matrix obtained from vibration test data. While the method proposed by Cao and Zimmerman constructs the Ritz vectors corresponding to the actual load pattern imposed on the structure, the proposed method is able to generate Ritz vectors from assumed load patterns as well. The residual flexibility, which is the contribution of unmeasured dynamic modes, is explicitly included in the proposed formulation. The effectiveness of the new extraction procedure is demonstrated using the data obtained from a vibration test of a grid-type bridge structure.

This paper is organised as follows: first, the analytical procedure of generating Ritz vectors is presented. Both the state-space-based method and the proposed flexibility matrix-based method are then described. We briefly describe the grid-type bridge model employed in the experimental study and the finite element model corresponding to the test structure. The proposed extraction procedure is then demonstrated using the experimental test data. Finally, this paper is concluded with a summary and discussions.

2. RITZ VECTOR EXTRACTION TECHNIQUES

In this section, we first review the analytical procedure for the generation of Ritz vectors [7]. Second, a state-space-based technique is described. A new extraction procedure based on a complete flexibility matrix constructed using measured vibration data is then presented.

2.1. ANALYTICAL PROCEDURE FOR GENERATING RITZ VECTORS

Let $\mathbf{M}$, $\mathbf{C}_\varsigma$, and $\mathbf{K}$ denote the mass, damping, and stiffness matrices of a N-dof system, respectively. Then, the equations of motion can be expressed as

$$\mathbf{M}\ddot{\mathbf{z}}(t) + \mathbf{C}_\varsigma\dot{\mathbf{z}}(t) + \mathbf{K}\mathbf{z}(t) = \mathbf{F}(t) \tag{1}$$

where $\mathbf{z}$, $\dot{\mathbf{z}}$, and $\ddot{\mathbf{z}}$ are the vectors of displacement, velocity and acceleration, respectively. $\mathbf{F}(t)$ is a $N \times 1$ vector representing the input force excitation. 'Load-dependent' Ritz vectors are generated by taking into account the 'spatial distribution' of the dynamic loading which is neglected in the generation of classical modal vectors. Assume that the dynamic loading $\mathbf{F}(t)$ can be separated into a spatial load vector $\mathbf{f}$ and a time function $u(t)$:

$$\mathbf{F}(t) = \mathbf{f}u(t). \tag{2}$$

The first Ritz vector is a static deformation caused by the spatial distribution of the dynamic load vector $\mathbf{f}$:

$$\mathbf{K}\bar{\mathbf{r}}_1 = \mathbf{f}: \quad \text{solve for } \bar{\mathbf{r}}_1 \ (= \tilde{\mathbf{r}}_1). \tag{3}$$

Then, the first Ritz vector is mass-normalised as

$$\mathbf{r}_1 = \frac{\tilde{\mathbf{r}}_1}{[\tilde{\mathbf{r}}_1^T \mathbf{M}\tilde{\mathbf{r}}_1]^{1/2}}. \tag{4}$$

The subsequent Ritz vectors are recursively generated. Assuming the mass matrix times the previous Ritz vector $\mathbf{M}\mathbf{r}_{s-1}$ to be a load, the recurrence relationship computes the next Ritz vector $\bar{\mathbf{r}}_s$:

$$\mathbf{K}\bar{\mathbf{r}}_s = \mathbf{M}\mathbf{r}_{s-1}: \quad \text{solve for } \bar{\mathbf{r}}_s. \tag{5}$$

The linear independence of Ritz vectors is achieved using the Gram–Schmidt ortho-gonalisation. That is, the current Ritz vector is mass-orthogonalised with respect to all the previous Ritz vectors:

$$\tilde{\mathbf{r}}_s = \bar{\mathbf{r}}_s - \sum_{t=1}^{s-1} (\mathbf{r}_t^T \mathbf{M} \bar{\mathbf{r}}_s)\mathbf{r}_t \tag{6}$$

Finally, the current Ritz vector is mass-normalised as

$$\mathbf{r}_s = \frac{\tilde{\mathbf{r}}_s}{[\tilde{\mathbf{r}}_s^T \mathbf{M} \tilde{\mathbf{r}}_s]^{1/2}}. \tag{7}$$

2.2. A STATE-SPACE-BASED METHOD

Recently, a procedure to extract Ritz vectors based on measured vibration test data has been proposed by Cao and Zimmerman [8]. This method involves a minimum rank realisation of state-space models from vibration test data. The second-order differential equations shown in equation (1) can be rewritten as the first-order differential equations in a number of ways. In classical control theory, the following state-space representation is often used (here, a single number of input is assumed for simplicity):

$$\dot{\mathbf{x}} = \mathbf{A}\mathbf{x} + \mathbf{B}u \tag{8}$$

where

$$\mathbf{A} = \begin{bmatrix} \mathbf{0} & \mathbf{I} \\ -\mathbf{M}^{-1}\mathbf{K} & -\mathbf{M}^{-1}\mathbf{C}_\varsigma \end{bmatrix}, \quad \mathbf{B} = \begin{bmatrix} \mathbf{0} \\ \mathbf{M}^{-1}\mathbf{f} \end{bmatrix} \quad \text{and} \quad \mathbf{x} = \begin{bmatrix} \mathbf{z} \\ \dot{\mathbf{z}} \end{bmatrix}. \tag{9}$$

When the response of a system is measured by the m output quantities $y(t)$ ($\in \Re^{m \times 1}$) using sensors such as accelerometer, the measurement vector $y(t)$ is related to the state vectors as follows:

$$\mathbf{y} = \mathbf{C}\mathbf{x} + \mathbf{D}u \tag{10}$$

where $\mathbf{C}$ is an $m \times 1$ output influence matrix and $\mathbf{D}$ is an $m \times 1$ gain matrix. Note that there exist an infinite number of state-space models that can be constructed from the same input and output relationship.

The state-space-based procedure starts with a minimum rank realisation of state matrices ($\hat{\mathbf{A}}$, $\hat{\mathbf{B}}$ and $\hat{\mathbf{C}}$) from the vibration data. In this study, the eigensystem realisation algorithm (ERA) is employed for the system realisation [9]. Note that the realised state matrices preserve the actual input–output characteristics regardless of the selection of state variables, $\mathbf{x}$. The state-space-based approach for the extraction of experimental Ritz vectors follows closely the analytical procedure for computing the Ritz vectors. The main difference is that the triple state-space matrices $\hat{\mathbf{A}}$, $\hat{\mathbf{B}}$ and $\hat{\mathbf{C}}$ are employed instead of the system matrices K, M, and the spatial load vector $\mathbf{f}$.

The static deformation vector $\bar{\mathbf{x}}_1$ subject to a load at the excitation point is computed by solving the following equation for $\bar{\mathbf{x}}_1$:

$$\hat{\mathbf{A}}\bar{\mathbf{x}}_1 = -\hat{\mathbf{B}}: \quad \text{solve for } \bar{\mathbf{x}}_1 \, (= \tilde{\mathbf{x}}_1) \tag{11}$$

where the input influence matrix $\hat{\mathbf{B}}$ contains the information of the load vector $\mathbf{f}$. Then, the first Ritz vector is normalised as

$$\mathbf{x}_1 = \frac{\bar{\mathbf{x}}_1}{[\bar{\mathbf{x}}_1^T \bar{\mathbf{x}}_1]^{1/2}}. \tag{12}$$

The subsequent Ritz vectors are recursively generated as follows:

$$\hat{\mathbf{A}}\bar{\mathbf{x}}_s = \mathbf{x}_{s-1}: \quad \text{solve for } \bar{\mathbf{x}}_s. \tag{13}$$

The linear independence among Ritz vectors is achieved by orthogonalising the current Ritz vector with respect to all the previous Ritz vectors:

$$\tilde{\mathbf{x}}_s = \bar{\mathbf{x}}_s - \sum_{t=1}^{s-1} (\mathbf{x}_t^{\mathrm{T}} \bar{\mathbf{x}}_s) \, \mathbf{x}_t. \tag{14}$$

Then, the current Ritz vector is normalised as

$$\mathbf{x}_s = \frac{\tilde{\mathbf{x}}_s}{[\tilde{\mathbf{x}}_s^{\mathrm{T}} \tilde{\mathbf{x}}_s]^{1/2}}. \tag{15}$$

Note that $\mathbf{x}_s$ is a Ritz vector in the state-space coordinate. Finally, the Ritz vector, which corresponds to the actual measurement points $\mathbf{r}_s$, is computed as

$$\mathbf{r}_s = \hat{\mathbf{C}}\mathbf{x}_s. \tag{16}$$

It should be noted that the normalisation and orthogonalisation procedures in the state-space method are not identical to those of the analytical generation procedure. Therefore, the Ritz vectors obtained from equation (16) should be normalised and orthogonalised with respect to the analytical mass matrix $\mathbf{M}$ in order to compare the experimental Ritz vectors with the analytical ones. In addition, matrix $\hat{\mathbf{A}}$ obtained from vibration tests often contains the 'noise' modes as well as the actual system modes. Therefore, the true modes corresponding to the actual system should be first distinguished before the Ritz vector extraction procedure. This process requires some engineering judgment. Various approaches to distinguish the true modes from the noise modes have been described in Juang [9].

2.3. A FLEXIBILITY MATRIX-BASED METHOD

In this section, we present a new extraction procedure of Ritz vectors based on a measured flexibility matrix. A close look at the analytical generation procedure reveals that the generation of Ritz vectors uses the flexibility matrix $\mathbf{G}$ (defined here as the inverse of the stiffness matrix) rather than the stiffness matrix itself. If the modal vectors are mass-normalised such that $\mathbf{V}^{\mathrm{T}}\mathbf{K}\mathbf{V} = \boldsymbol{\Omega}$ and $\mathbf{V}^{\mathrm{T}}\mathbf{M}\mathbf{V} = \mathbf{I}$, the flexibility matrix can be represented with the modal parameters [10]:

$$\mathbf{G} = \mathbf{K}^{-1} = \mathbf{V}\boldsymbol{\Omega}^{-1}\mathbf{V}^{\mathrm{T}} \tag{17}$$

where $\boldsymbol{\Omega}$ is the diagonal eigenvalue matrix and $\mathbf{V}$ is the corresponding eigenvector (modal vector) matrix.

In most experimental modal analyses, only a few lower modal frequencies and modal vectors are identified. For this case, the flexibility matrix is divided into the *modal flexibility*, which is formed from the estimated frequencies and modal vectors, and the *residual flexibility* formed from the residual modes:

$$\mathbf{G} = \mathbf{G}_m + \mathbf{G}_r = \mathbf{V}_m\boldsymbol{\Omega}_m^{-1}\mathbf{V}_m^{\mathrm{T}} + \mathbf{V}_r\boldsymbol{\Omega}_r^{-1}\mathbf{V}_r^{\mathrm{T}} \tag{18}$$

where the subscripts m and r denote the modal and residual quantities, respectively. Here, the modal flexibility $\mathbf{G}_m$ is easily constructed using the measured natural frequencies and modal vectors. The residual flexibility $\mathbf{G}_r$ is the contribution of the unmeasured

dynamic modes to the full flexibility matrix. In general, the contribution of lower modes, which are normally estimated in experimental modal analyses, is more significant than those of higher modes because the contribution of each mode is inversely proportional to the magnitude of the corresponding natural frequencies. Deobling *et al.* [10] report that the contribution of the residual flexibility matrix is generally about 3–10% of the complete flexibility matrix. However, as shown in later examples, the contribution of the residual flexibility cannot be neglected in the extraction procedure of Ritz vectors.

The residual flexibility is constructed using a residual function $\mathbf{R}(\omega)$, which is computed by subtracting the reconstructed response of the identified modes from the measured frequency response functions (FRFs) $\mathbf{H}(\omega)$:

$$\mathbf{R}(\omega) = \mathbf{H}(\omega) + \omega^2 \, \mathbf{V}_m (\mathbf{\Omega}_m - \omega^2 \, \mathbf{I})^{-1} \, \mathbf{V}_m^{\mathrm{T}} = -\mathbf{G}_r \omega^2. \tag{19}$$

Curve-fitting $\mathbf{R}(\omega)$ over a set of frequency samples ($\omega \in \omega_{set}$) yields an estimate of the residual flexibility

$$\mathbf{G}_r = - \sum_{\omega \in \omega_{\mathrm{set}}} \frac{\mathbf{R}(\omega)}{\omega^2}. \tag{20}$$

In this paper, $\mathbf{H}(\omega)$ and $\mathbf{R}(\omega)$ are assumed to be squared matrices. That is, individual modal testing is conducted by applying an impulse excitation force to a dof and the excitation is repeated for all measured dofs. Doebling *et al.* [10] discuss the extraction of a complete flexibility when the number of excitation points are less than that of the response points. While damping is not included in the formulation of the residual flexibility, equation (19) can be easily modified to take into account the damping.

From the measured flexibility matrix $\mathbf{G}$ ($= \mathbf{G}_m + \mathbf{G}_r$) and the analytical mass matrix $\mathbf{M}$, the first Ritz vector can be computed as

$$\bar{\mathbf{r}}_1 = \mathbf{G}\mathbf{f} \tag{21}$$

where $\mathbf{f}$ is the spatial load distribution vector defined in equation (2). The first Ritz vector is, then, mass-normalised as

$$\mathbf{r}_1 = \frac{\tilde{\mathbf{r}}_1}{[\tilde{\mathbf{r}}_1^{\mathrm{T}} \mathbf{M} \tilde{\mathbf{r}}_1]^{1/2}}. \tag{22}$$

The subsequent Ritz vectors are recursively generated in a similar fashion to equation (5). The only difference is that the flexibility matrix is directly constructed from the test data instead of inverting the analytical stiffness matrix. The orthogonalisation and mass-normalisation procedures are identical to equations (6) and (7).

It is worthwhile to compare the flexibility-based extraction procedure with the state-space based procedure. In the state-space method, the input influence matrix $\hat{\mathbf{B}}$ in equation (11) is estimated using the information of the experimentally applied load. While the state-space-based method only identifies Ritz vectors corresponding to the specific excitation pattern used in the actual modal testing, the flexibility-based method is able to generate Ritz vectors with arbitrary load patterns as well. That is, the spatial load distribution vector $\mathbf{f}$ in equation (21) can be arbitrarily assigned to generate different sets of Ritz vectors. Furthermore, the contribution of the residual flexibility is not included in the state-space-based method. (The influence of the residual flexibility on the accuracy of the estimated Ritz vectors will be addressed in Section 5.) Note that both methods require an appropriate approximation for the mass matrix. However, for problems that stiffness changes are the

main concern as in the case for damage detection, the exact estimation of the mass matrix is not necessarily an important issue. One will be more likely interested in the change of Ritz vectors caused by stiffness perturbation. It should also be pointed out that Alvin [11] has presented a theory to transform the realised state-space models into the corresponding second-order structural parameters such as stiffness, mass and damping matrices based on an objective normalisation of physical-coordinated modal vectors. Using these directly computed stiffness and mass matrices, an arbitrary set of Ritz vectors could also be extracted in theory.

3. AN EXPERIMENTAL BRIDGE MODEL

For this study, a grid-type bridge model has been constructed and tested at the Hyundai Institute of Construction Technology (HICT), Korea (Fig. 1). The steel bridge model consists of two parallel girders and six evenly spaced cross-beams connecting the two girders. The girders are steel rectangular tubes and the cross-beams are C-shape members. Using impact excitations, we extract Ritz and modal vectors from the vibration response of this test structure.

A SA-390 signal analyzer with four channels is used for the analog-to-digital conversion of accelerometer signals and the fast Fourier transform (FFT) calculation. Data acquisition parameters are specified such that a frequency response function (FRF) in the range of 0–100 Hz could be estimated. Each spectrum is computed by averaging three 8 s long time histories. A total of 2048 points are sampled for a 8 s time period and this sampling rate produces a frequency resolution of 0.125 Hz. An exponential window is applied to all measured time histories prior to the FFT calculation.

For measurements, a Dytran 5801A4 impact hammer and three Dytran 3100B accelerometers with a normal sensitivity of 100 mV/g are used. The excitation is applied at each node as shown in Fig. 2. The sensors measure the vertical accelerations at the 12 nodes as indicated in Fig. 2. Note that since the SA-390 data acquisition system has only four channels and there are three accelerometers, the first channel is always connected to the input hammer and the remaining three channels are connected to three accelerometers. To complete one set of modal test, the hammer excitation is repeated 12 times at one point and the three accelerometers are moved from one set of three nodes to another set of three nodes after every three excitations. Note that each FRF is computed by averaging three response time histories, and there are 12 measurement points and three accelerometers.
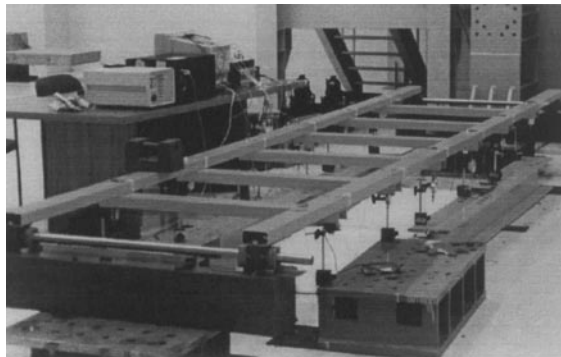

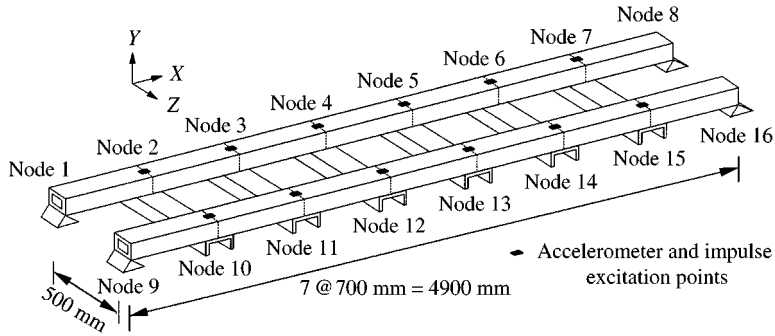Figure 1. An overview of a grid-type bridge structure.

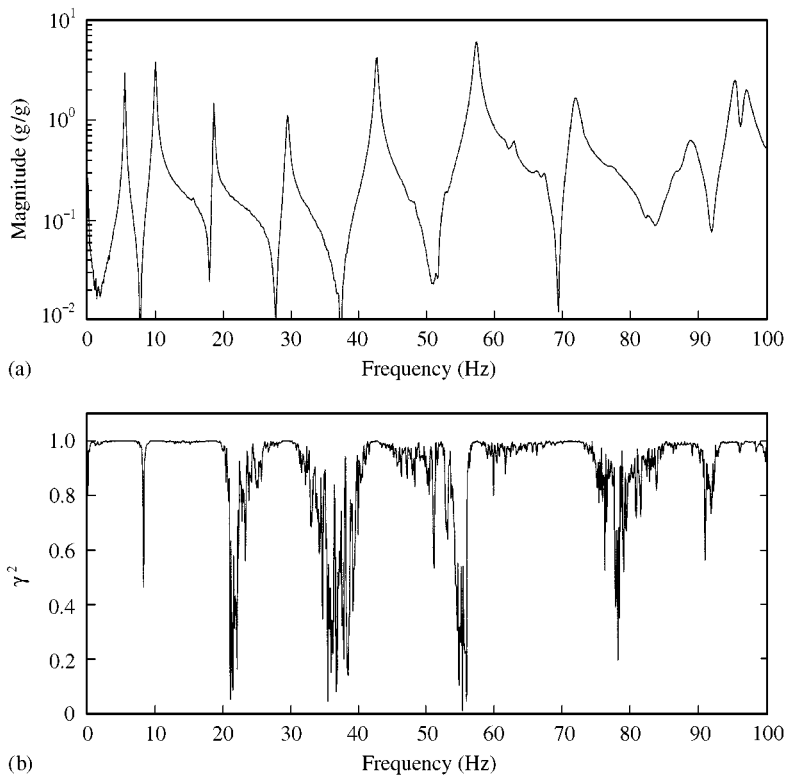Figure 2. Configuration of a grid-type bridge model.

Figure 3. A typical FRF & coherence function of the grid-type bridge model. (a) A FRF of node 5 with node 4 input. (b) A coherence function of node 5 with node 4 input.

The rational polynomial technique is employed to extract the first six natural frequencies and the corresponding modal vectors from the recorded FRFs [12]. Figure 3 shows a typical FRF and coherence function of the test structure. Figure 3(a) is a FRF obtained at node 5 when the structure is excited at node 4. Figure 3(b) presents the corresponding coherence function. Figure 3(b) shows that the value of the coherence function is close to unity at the resonance frequencies, which indicates that the output signals from the sensors are reasonably strong as compared to the noise levels.
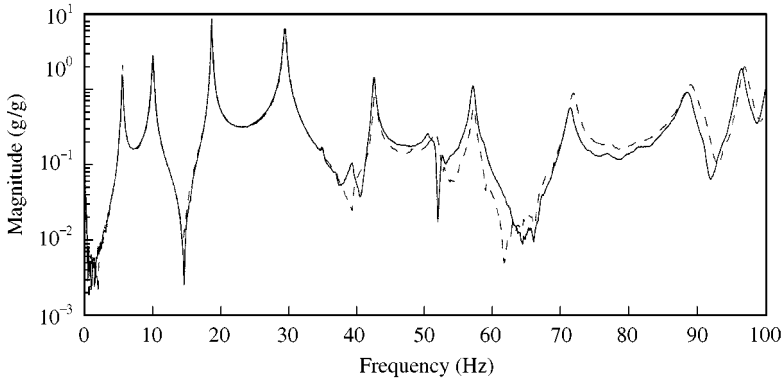
Figure 4. A reciprocity check of the grid-type bridge model: —— excitation: node 3, response: node 14; – – –
excitation: node 14, response: node 3.

To validate the linearity assumption of the structure response, a reciprocity check has
been conducted. Figure 4 compares the FRFs obtained at node 3 with an input at node 14
and at node 14 with an excitation at node 3. For an ideal linear structure, these two FRFs
should be identical. For the grid structure, the linearity assumption seems valid up to the
fourth mode but the difference between the FRFs becomes noticeable after 40 Hz.

4. ANALYTICAL MODELLING OF THE TEST STRUCTURE

A finite element (FE) model for the grid-type bridge structure is constructed using
23-dimensional beam elements. As shown in Fig. 2, a girder segment between two nodes or
a cross-beam is modelled as a single element. An elastic modulus of 2.0×10^5 MPa, a mass
density of 7850 kg/m³, and a Poission ratio of 0.2 are specified for the model. Since the
accelerometers measure only the vertical movement of the structure, the lateral dofs are not
included in the analytical model. Therefore, each node of an element has two translational
dofs and three rotational dofs. The model has a total of 64 dofs including four rotational
dofs at the boundary. Both ends of the beam are modelled as simple pinned connections.

A pinned connection is modelled by a ball bearing with a 35 mm diameter in the
experimental set-up. Based on a preliminary vibration test, the boundary conditions appear
to be less accurately modelled. The boundary conditions are then modified by introducing
rotational springs at the rotational dofs of the boundaries. Furthermore, additional springs
are added to the rotational dofs at both end of the cross-beams to simulate the bolted
connection between the girders and the cross-beams. After these modifications, the relative
errors of the first six natural frequencies between the analytical model and the test structure
fall within 4%.

Table 1 compares the natural frequencies of the analytical model computed after model
updating with the experimental frequencies. Here, the experimental frequency $\hat{\omega}$ is a mean
value of the 12 frequencies estimated with an impact load applied at nodes 2–7, and 10–15,
respectively. The damping ratios for the first six modes are also estimated: 0.8725, 0.9780,
0.3420, 0.6151, 0.4231, and 0.4981%.

Figure 5 displays the analytical and experimental modal vectors of the first six modes. All
figures are plotted in the global X–Y plane of Fig. 2, viewing the structure from the side. As
for the scaling of the modal or Ritz vectors, a mass normalisation is conducted. However,

TABLE 1

Comparison of the analytical and experimental natural frequencies

Mode	Frequency (Hz)		Relative error (%)
	Analytical	Experimental	
1st bending	5.4488	5.5780	2.32
1st torsion	10.1494	10.0610	0.88
2nd bending	19.1841	18.6441	2.90
2nd torsion	30.6216	29.4503	3.98
3rd bending	41.6086	42.6292	2.39
3rd torsion	54.9704	57.2512	3.98

Error $= 100 \times |\omega - \hat{\omega}|/\hat{\omega}$: ω and $\hat{\omega}$ are analytical and experimental frequencies.
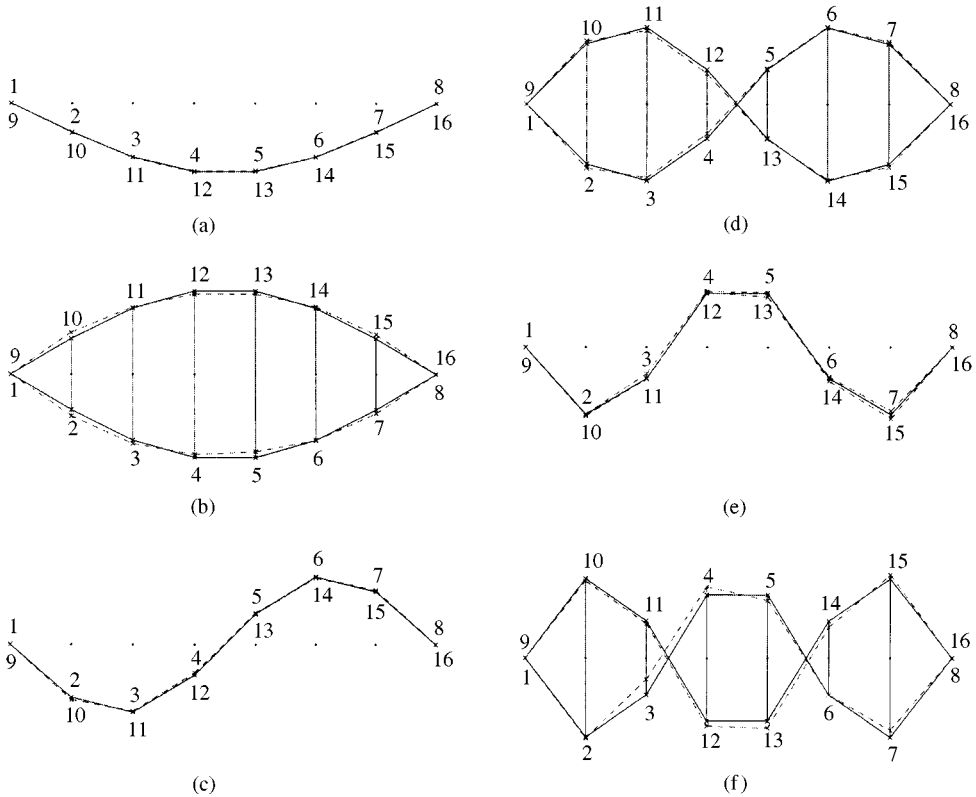
Figure 5. Comparison of analytical and experimental modal vectors. (a) Modal vector 1; (b) Modal vector 2; (c) Modal vector 3; (d) Modal vector 4; (e) Modal vector 5; (f) Modal vector 6: —— analytical; – – – experimental.

since the dofs of the analytical model do not coincide with the dofs of the experimental modal vectors, a reduced analytical mass matrix is first computed using the Guyan condensation procedure. Both the analytical and experimental vectors are normalised with respect to the reduced mass matrix. Errors arisen from the model reduction are found to be

minimum since the inertial forces associated with the omitted rotational and axial dofs (slave dofs) are negligible in this example.

5. EXPERIMENTAL VERIFICATION

The new extraction procedure for Ritz vectors is demonstrated using the vibration data obtained from the test structure. Special focus is placed on the influence of the residual flexibility on the accuracy of extracted Ritz vectors. Figure 6 compares the first six Ritz vectors estimated by the flexibility-based method with the corresponding Ritz vectors computed from the FE model. Imaginary point loads are simultaneously applied to nodes 2 and 13 (upward point load at node 2 and downward point load at node 13), and the corresponding Ritz vectors are generated. A complete flexibility matrix, including the modal and residual flexibility matrices estimated from the measured FRFs, is employed for the extraction of Ritz vectors. Figure 6 shows a good agreement between the analytical and experimental Ritz vectors. The first Ritz vector is equivalent to a static deflection pattern observed when the unit loads are applied at nodes 2 and 13. Note that the discrepancy between the analytical and experimental Ritz vectors increases for higher Ritz vectors.

To investigate the influence of the residual flexibility, Fig. 7 shows the experimental Ritz vectors obtained by only using the measured modal flexibility. Comparison of Figs. 6 and
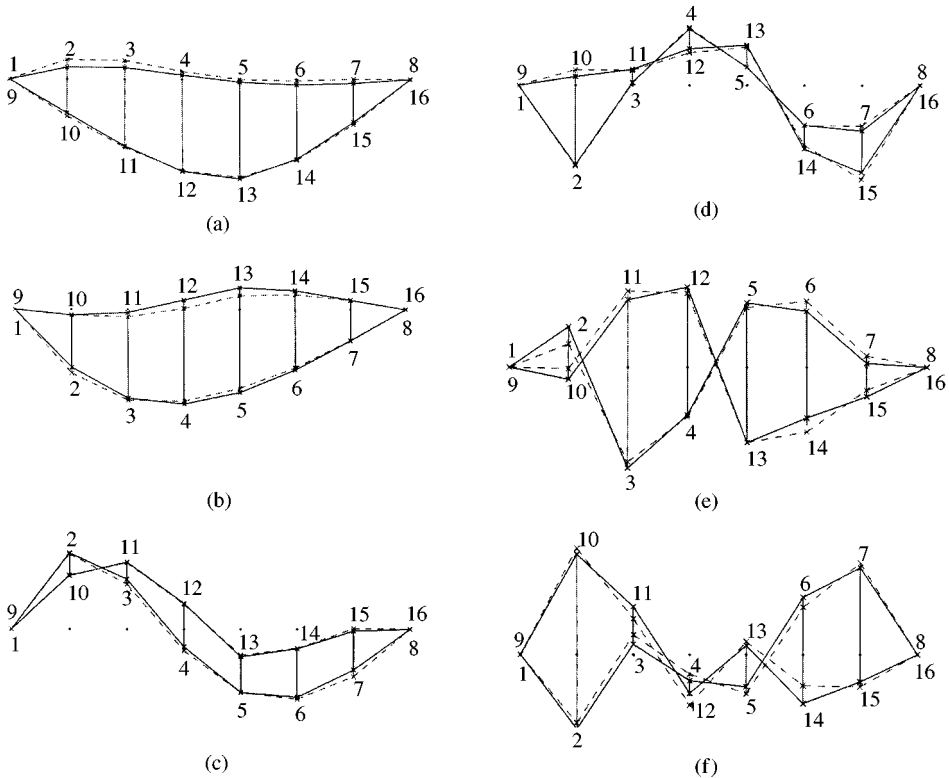

Figure 6. Comparison of analytical and experimental Ritz vectors (using a complete flexibility, $\mathbf{G} = \mathbf{G}_m + \mathbf{G}_r$). (a) Ritz vector 1; (b) Ritz vector 2; (c) Ritz vector 3; (d) Ritz vector 4; (e) Ritz vector 5; (f) Ritz vector 6: ——— analytical; – – – experimental.
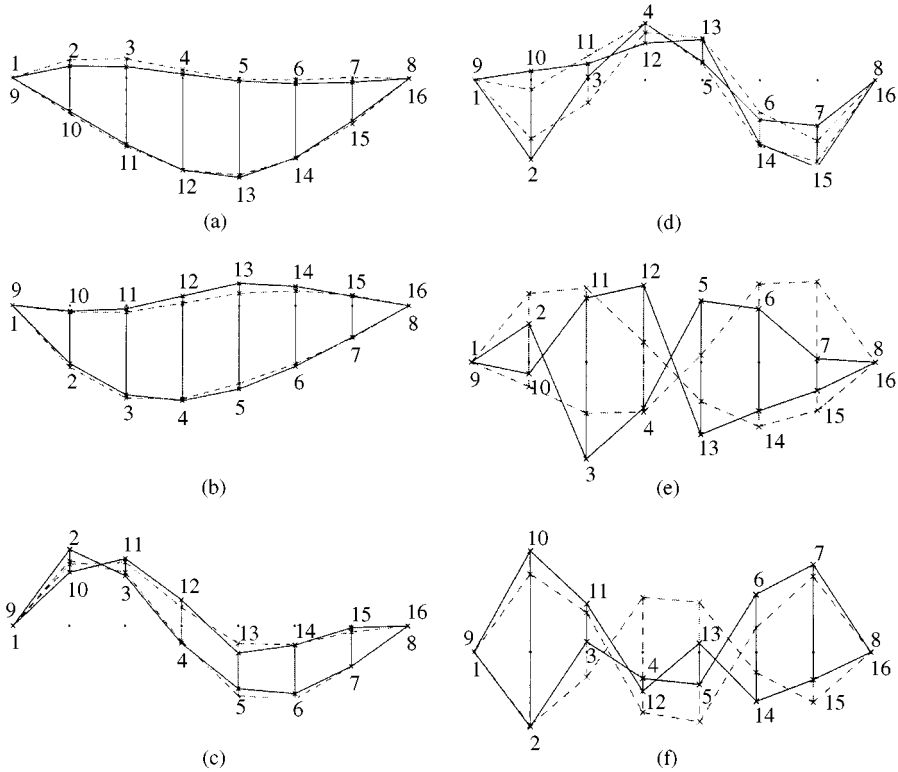
Figure 7. Comparison of analytical and experimental Ritz vectors (using only a modal flexibility, $\mathbf{G} = \mathbf{G}_m$). (a) Ritz vector 1; (b) Ritz vector 2; (c) Ritz vector 3; (d) Ritz vector 4; (e) Ritz vector 5; (f) Ritz vector 6: —— analytical; − − − experimental.

TABLE 2

MAC values between analytical and experimental Ritz vectors

			i for MAC(i, i)			
G	1	2	3	4	5	6
$\mathbf{G}_m + \mathbf{G}_r$	0.9947	0.9930	0.9971	0.9956	0.9754	0.9720
$\mathbf{G}_m$	0.9946	0.9930	0.9876	0.9099	0.3932	0.0211

MAC$(i, j) = (\mathbf{r}_i^{\mathrm{T}} \mathbf{M} \hat{\mathbf{r}}_j)^2 / [(\mathbf{r}_i^{\mathrm{T}} \mathbf{M} \mathbf{r}_j)(\hat{\mathbf{r}}_i^{\mathrm{T}} \mathbf{M} \hat{\mathbf{r}}_j)]$, $\mathbf{r}_i$ = analytical and $\hat{\mathbf{r}}_j$ = experimental.

7 reveals that the inclusion of the residual term significantly improves the accuracy of higher Ritz vectors. More quantitative analysis is presented in Table 2, where the modal assurance criterion (MAC) value is defined as follows:

$$\text{MAC}(i, j) = (\mathbf{r}_i^{\mathrm{T}} \mathbf{M} \hat{\mathbf{r}}_j)^2 / [(\mathbf{r}_i^{\mathrm{T}} \mathbf{M} \mathbf{r}_i)(\hat{\mathbf{f}}_j^{\mathrm{T}} \mathbf{M} \hat{\mathbf{r}}_j)] \tag{23}$$

where $\mathbf{r}_i$ and $\hat{\mathbf{r}}_j$ are the analytical and experimental Ritz vectors, respectively.

TABLE 3

MAC values for different load patterns (using the complete flexibility, $\mathbf{G}_m + \mathbf{G}_r$)

	i for MAC(i, i)					
Node	1	2	3	4	5	6
2	0.9944	0.9929	0.9980	0.9931	0.9888	0.9805
3	0.9983	0.9964	0.9955	0.9945	0.9485	0.9657
4	0.9994	0.9974	0.9966	0.9948	0.9857	0.9900
5	0.9994	0.9966	0.9903	0.9907	0.9761	0.9656
6	0.9989	0.9965	0.9967	0.9976	0.9755	0.9824
7	0.9954	0.9952	0.9917	0.9800	0.9717	0.9731
10	0.9937	0.9925	0.9950	0.9785	0.9697	0.9737
11	0.9984	0.9956	0.9978	0.9978	0.9790	0.9849
12	0.9995	0.9965	0.9932	0.9929	0.9825	0.9764
13	0.9996	0.9970	0.9968	0.9970	0.9885	0.9877
14	0.9993	0.9970	0.9951	0.9958	0.9542	0.9635
15	0.9963	0.9953	0.9956	0.9935	0.9866	0.9819

MAC$(i, j) = (\mathbf{r}_i^{\mathrm{T}} \mathbf{M} \mathbf{r}_j)^2 / [(\mathbf{r}_i^{\mathrm{T}} \mathbf{M} \mathbf{r}_j)(\hat{\mathbf{r}}_i^{\mathrm{T}} \mathbf{M} \hat{\mathbf{r}}_j)]$, $\mathbf{r}_i$ = analytical and $\hat{\mathbf{r}}_j$ = experimental.

TABLE 4

MAC values for different load patterns (using the modal flexibility, $\mathbf{G}_m$)

	i for MAC(i, i)					
Node	1	2	3	4	5	6
2	0.9944	0.9920	0.9913	0.9429	0.7541	0.3560
3	0.9982	09958	0.9887	0.9502	0.4777	0.0848
4	0.9993	0.9967	0.9678	0.9262	0.7802	0.3623
5	0.9994	0.9958	0.9472	0.8818	0.6782	0.2588
6	0.9989	0.9962	0.9909	0.9627	0.5722	0.1649
7	0.9952	0.9933	0.9779	0.9019	0.6498	0.2654
10	0.9938	0.9910	0.9827	0.9096	0.6753	0.2651
11	0.9984	0.9952	0.9925	0.9621	0.5631	0.1578
12	0.9995	0.9958	0.9569	0.8997	0.7208	0.2973
13	0.9996	0.9964	0.9630	0.9139	0.7431	0.3377
14	0.9992	0.9965	0.9895	0.9566	0.5213	0.1140
15	0.9962	0.9938	0.9847	0.9306	0.7229	0.3424

MAC$(i, j) = (\mathbf{r}_i^{\mathrm{T}} \mathbf{M} \mathbf{r}_j)^2 / [(\mathbf{r}_i^{\mathrm{T}} \mathbf{M} \mathbf{r}_j)(\hat{\mathbf{r}}_i^{\mathrm{T}} \mathbf{M} \hat{\mathbf{r}}_j)]$, $\mathbf{r}_i$ = analytical and $\hat{\mathbf{r}}_j$ = experimental.

Although not presented here, the state-space-based method basically produces the same results as the proposed method with only using the modal flexibility. Furthermore, as mentioned earlier, only the flexibility-based method allows generating Ritz vectors from any fictitious load patterns as well as the actual load pattern applied during the tests.

In Table 3, the experimental Ritz vectors corresponding to a point load at nodes 2–7 and 10–15 are extracted, and the comparison of MAC values with the corresponding analytical Ritz vectors are presented. Again, the measured complete flexibility is used for all cases in the table. For brevity, only the diagonal components of the MAC values are shown in the table. The result indicates that the Ritz vectors can be successfully generated from all the load patterns imposed.

Next, the Ritz vectors are estimated using only the modal flexibility, and the MAC values are presented in Table 4. For all cases, the MAC values between the analytical and experimental Ritz vectors fall below 0.8 after the fourth Ritz vectors. The inclusion of the residual flexibility matrix into the extraction procedure allows the contribution of higher residual modes into experimentally estimated Ritz vectors significantly improving the accuracy of the estimated Ritz vectors.

6. SUMMARY AND DISCUSSIONS

In this paper, a new procedure has been proposed to extract load-dependent Ritz vectors using a statically complete flexibility matrix. First, modal flexibility and residual flexibility matrices are estimated from measured FRFs. Then, Ritz vectors are recursively generated using the flexibility matrix constructed.

The procedure is successfully demonstrated using an experiment of a grid-type bridge structure. Particularly, the influence of the residual flexibility on the extracted Ritz vectors is investigated. The proposed method has at least two advantages over the state-space method: (1) the inclusion of the residual flexibility significantly improves the accuracy of the estimated Ritz vectors, and (2) the proposed method is able to generate Ritz vectors from any arbitrary load patterns. The increased amount of information and better sensitivity to structural parameter changes, which are achievable by multiple loading and careful selection of load patterns, could improve the results of damage detection, test-analysis correlation, model refinement and system identification.

Using the Ritz vectors extracted with the procedure described here, Sohn and Law [13] have applied and analysed the various damage cases introduced to the grid-type bridge structure presented in this study. Damage diagnoses of the grid-type bridge structure indicates that the employment of Ritz vectors provides better indication of the actual damage locations than using the modal vectors. The reason is that, using appropriate load patterns, Ritz vectors can be made more sensitive to damage than modal vectors. The superior performance of Ritz vectors over modal vectors attributes to (1) the better sensitivity of Ritz vectors over modal vectors and (2) the increase amount of information obtained by employing multiple load patterns.

There have been continuing interest in the application of Ritz vectors for experimental dynamics problems. Rhee [14] shows how Ritz vectors can be used to effectively characterise the changes of the system dynamic properties caused by localised non-proportional damping effects and/or structural perturbation. Model reduction and mode shape expansion techniques are further developed for model updating purpose based on experimentally extracted Ritz vectors. These techniques are demonstrated using experimental data obtained from an eight dof mass–spring system. To verify the feasibility and accuracy of the experimental Ritz vectors, Zimmerman [15] utilised the dynamic and static test data obtained from a space shuttle vertical stabilizer. Compared to static test data, accurate Ritz vectors were extracted from a modal survey test using both accelerometers and a laser scanning vibrometer. Then, a matrix update approach using the measured Ritz vectors is conducted to update an FE model and to estimate the location and extent of damage. The proposed Ritz vector extraction procedure described in this paper could find many applications in system identification and damage detection problems.

REFERENCE

1. B. NOUR-OMID and R. W. CLOUGH 1984 *Earthquake Engineering and Structural Dynamics* **12**, 565–577. Dynamics analysis of structures using Lanczos coordinates.
2. E. L. WILSON, M. W. YUAN and J. M. DICKEN 1982 *Earthquake Engineering and Structural Dynamics* **10**, 813–821. Dynamic analysis by direct superposition of Ritz vectors.
3. G. H. GOLUB and C. F. VAN LOAN 1996 *Matrix Computations*. Maryland: The Johns Hopkins University Press.
4. C. M. M. CAREY, G. H. COLUB and K. H. LAW 1994 *International Journal for Numerical Methods in Engineering* **37**, 2857–2883. Lanczos-based method for structural dynamic reanalysis problems.
5. T. T. CAO and D. C. ZIMMERMAN 1997 *Proceedings of the 15th International Modal Analysis Conference*, *Orlando*, FL, 1319–1324. Application of load-dependent Ritz vectors in structural damage detection.
6. H. SOHN and K. H. LAW 2000 *Probabilistic Engineering Mechanics* **15**, 139–153. Application of load-dependent Ritz vectors to Bayesian probabilistic damage detection.
7. P. LEGER, E. L. WILSON and R. W. CLOUGH 1986 *Technical Report UCB/EERC-86/04*, *Earthquake Engineering Research Center*, *University of California Berkeley*, *Berkeley*, *CA*. The use of load-dependent Ritz vectors for dynamic and earthquake analyses.
8. T. T. Cao and D. C. Zimmerman 1997 *Proceedings of the 15th International Modal Analysis Conference*, *Orlando*, *FL*, 1036–1042. A procedure to extract Ritz vectors from dynamic testing data.
9. J. N. JUANG 1994 *Applied Systems Identification*. Englewood Cliffs, NJ: Prentice-Hall.
10. S. W. DOEBLING, L. D. PETERSON and K. F. ALVIN 1996 *American Institute of Aeronautics and Astronautics* **34**, 1678–1685. Estimation of reciprocal residual flexibility from experimental modal data.
11. K. F. ALVIN 1994 *American Institute of Aeronautics and Astronautics* **32**, 397–406. A second-order structural identification procedure via state-space based system identification.
12. M. H. RICHARDSON and D. L. FORMENTI 1982 *Proceedings of the 1st International Modal Analysis Conference*, *Orlando*, *FL*, 167–181. Parameter estimation form frequency response measurements using rational fraction polynomials.
13. H. SOHN and K. H. LAW 2001 *Journal of Engineering Mechanics*, *ASCE*. Damage diagnosis using experimental Ritz vectors (accepted for publication).
14. W. RHEE 2000 *Ph.D. Dissertation*, *Texas Tech University*, *Lubbock*, *TX*. Linear and nonlinear model reduction in structural dynamics with application to model updating.
15. D. C. ZIMMERMAN 1999 *Key Engineering Materials* **167–168**, 76–90. Looking into the crystal ball: the continued need for multiple viewpoints in damage detection.